Pulsed Thermal NDT of Material Discontinuities by Using the Concept of Equivalent Effusivity/Diffusivity Variations

A.O. Siddiqui[1a], Y.L.V.D. Prasad[1], V.P. Vavilov[2], D. Yu. Kladov[2]

[1]Advanced Systems Laboratory, Kanchanbagh P.O., Hyderabad 500058
[2] National Research Tomsk Polytechnic University 634050 Tomsk, Lenin Av., 30, Russia
[a]*Email: ahmedovais.asl@gov.in*

Abstract

Subsurface material discontinuities lead to local variations of apparent thermal effusivity and diffusivity. The analysis of equivalence between such variations and defect parameters is useful from both theoretical and practical points of view. Classical heat conduction solutions contain effusivity/diffusivity as important parameters, which can be used for defect characterization. Also, conversion of temperature images into maps of thermal propertiesmay enhance defect visibility, for example, by transiting from the temperature domain into the time domain, as it appears in the case of diffusivity measurement. A 60J impact damage in carbon fiber reinforced polymer is characterized by effusivity/diffusivity variation from 20 to 40 %.

Keywords: *Nondestructive testing, Infrared thermography, Defect, Diffusivity, Effusivity*

1.Introduction:

In pulsed thermal nondestructive testing (NDT), subsurface defects of materials are detected by analyzing dynamic temperature distributions on the surface of test samples excited by a pulse or waves of thermal energy. Several types of thermal stimulation can be used but typically it is performed by means of flash tubes and halogen lamps [1]. In one-sided tests, front (F) surface temperature signals, which appear over defects, essentially decay by amplitude and delay in time with increasing defect depth *l*, while on the rear (R) surface temperature signals and their evolution in time are weakly dependent on *l*, see the test scheme in figure 1. In the last decade, thermal NDT appeared as a powerful tool for evaluating quality of composite materials, see the recent review [2] and some topical papers [3-5].
Classical analytical solutions of heat conduction in solids are typically one-dimensional (1D) and involve material thermal properties as solution parameters, namely, thermal effusivity*e* and thermal diffusivity *a*. The concept of pulsed thermal NDT accepted in this study assumes that a discontinuity-like defect phenomenologically can be considered as a local variation of the above-mentioned parameters Δe(F-surface procedure) and Δa(R-surface procedure). This concept wasearlier used for analyzing severity of impact damage in carbon fiber reinforced polymer (CFRP) composites [6,7]. The investigations were conducted on large series of CFRP samples which contained impact damages in a wide range of energy, while the samples were subjected to temperature cycling tests and moistening.
In this study we, first, analyze the theoretical aspects of the relationship between discontinuity-like defects and thermal property variations by using 3D modeling and afterwards supply an experimental illustration for both one- and two-sided inspection of impact damage in CFRP.

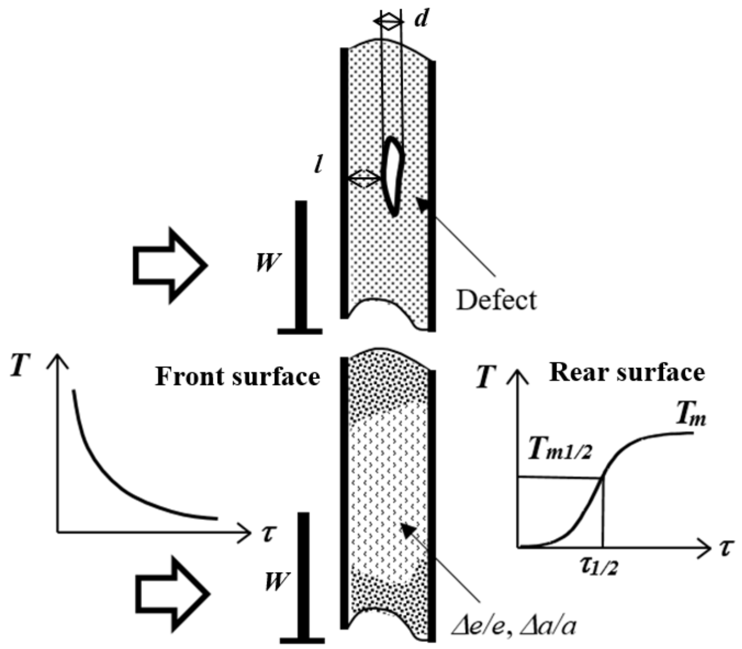

Fig.1 One-and two-sided thermal NDT procedures: equivalence between defects and apparent variations of thermal properties

2.Theory: back to basics

The Dirac-pulse heating of an adiabatic homogeneous plate is described with the two well-known expressions:

$T = \frac{Wa}{\lambda L}\ [1 + 2\sum_{n=1}^{\infty} e^{-n^2\pi^2 Fo}]$ on the F-surface;

$T = \frac{Wa}{\lambda L}\ [1 + 2\sum_{n=1}^{\infty}(-1)^n e^{-n^2\pi^2 Fo}]$, on the R-surface (1)

Here: W is the absorbed energy, λ is the thermal conductivity,$a$is the thermal diffusivity, L is the plate thickness, and $Fo = a\tau/L^2$ is the Fourier number. The plots of the functions above are schematically shown in figure1.The three material thermal properties (C, the heat capacity, ρ, the density and thermal conductivity $\lambda = C\rho a$) cannot be determined without having measured absorbed energy; note that the dimensions of these quantities contain energy in Joules. Oppositely, thermal diffusivity$a$, of which dimension is m^2/s, can be evaluated by analyzing some inflection points in the R-surface$T^R(\tau)$ functions. Such inflection points naturally appear in $T^R(\tau)$ curves, while the processing of F-surface $T^F(\tau)$ curves requires using some mathematical "tricks", such as non-linear fitting [8, 9]. Reliability of the corresponding estimates on the R-surface is typically higher than those on the F-surface. Physically, this is explained by the fact, that in a two-sided procedure the heat energy travels across a sample thus being affected by material bulk properties, unlike a one-sided procedure where the influence of material properties on the surface temperature strongly decays with increasing depth.

It is worth noting that Eqs. (1) contain the infinite number of exponential members which are often interpreted as pulsed thermal waves travelling between the F- and R-surfaces of the plate. Front-surface solutions become much simpler if a plate can be replaced with a semi-infinite body, of which Dirac-pulse heating is described by the equation:

$T = \frac{W}{e\sqrt{\pi}}\frac{1}{\sqrt{\tau}}$,(2)

Where $e = \sqrt{C\rho\lambda}$ is the effusivity, or thermal inertia. Obviously, the determination of absolute values of

$e = W/(T\sqrt{\pi\tau})$(3)

is also linked to measuring absorbed energy but in thermal NDT one often analyzes the temporal behavior of the $e/W = 1/(T\sqrt{\pi\tau})$function. It is also worth noting that any plate behaves as the respective semi-infinite body at shorter observation times that follows from Eq. (1) at short Fo times. It is important noting that experimentally determined e values are apparent and vary in time.

In a two-sided procedure, thermal diffusivity is typically determined by using the Parker formula [10]:

$$a = \frac{0.139L^2}{\tau_{1/2}} (4)$$

where$\tau_{1/2}$ is the so-called half-rise-time easily determined in a $T^R(\tau)$ curve, see the plot in figure 1.

3. Effusivity and diffusivity *vs.* subsurface defect parameters – sensitivity analysis

In this section we analyze how the presence of subsurface defects changes apparentlocal thermal properties of a material under test: effusivity in a one-sided procedure and diffusivity in a two-sided procedure.The underlying concept is to model some defect situations where air-filled defects having different thickness d and located at different depths l modify the values of local apparent effusivitycalculated by Eq. (3) and diffusivity calculated by Eq. (4) to compare to the respective “non-defect” values.

3.1 Test model description

Two CFRP sampleswith the thickness of 1 and 6 mm were analyzed in both one- and two-sided procedures. The heating time was 1 second and the heating power - 10 kW/m^2. Four synthetic image sequences have been produced to determine variations in apparent local effusivity and diffusivity, i.e. at the points located over the centers of the air-filled defects. Defect depth and thickness varied to study influence of these parameters on thermal property variations. Since defect lateral dimensions greater than 10 mm weakly influence surface temperature signals [1], in this model only 10x10 mm defects have been analyzed according to the scheme in figure 2a. The examples of apparent effusivity and diffusivity maps are presented in figure 2b, c.

It is worth noting again the principal difference between maps of effusivity and diffusivity. Diffusivity is a unique integral parameter which characterizes a sample in a particular heating procedure. Diffusivity values are calculated by processing a whole synthetic sequence. Effusivity can be regarded as a unique parameter only if Dirac-pulse heating of an adiabatic semi-infinite body is involved. In our case, we deal with square-pulse heating of non-adiabatic plates, therefore, effusivity is to be calculated for each single image in a synthetic sequence varying from image to image through the sequence. In the analysis below, effusivity variation for each defect has been calculated at the time when a differential temperature signal for this particular defect achieves a maximum value.

For the 1 mm-thick sample, the synthetic sequence included 150 images with the acquisition interval being 0.1s; whereas, for 6 mm-thick sample, the synthetic sequence included 100 images with the acquisition interval being 1s.

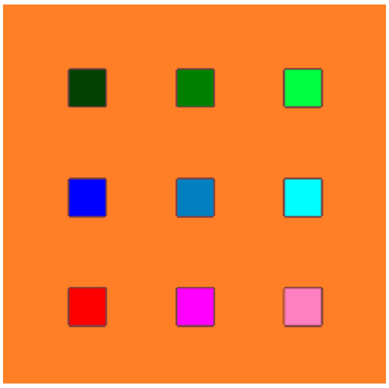

Fig.2a Scheme of defects

Sample 1: L=1 mm: defect depth 0.2, 0.5 and 0.8 mm, defect thickness 0.05, 0.10 and 0.15 mm

Sample 2: L=6 mm: defect depth 1, 3 and 5 mm, defect thickness 0.05, 0.10 and 0.20 mm

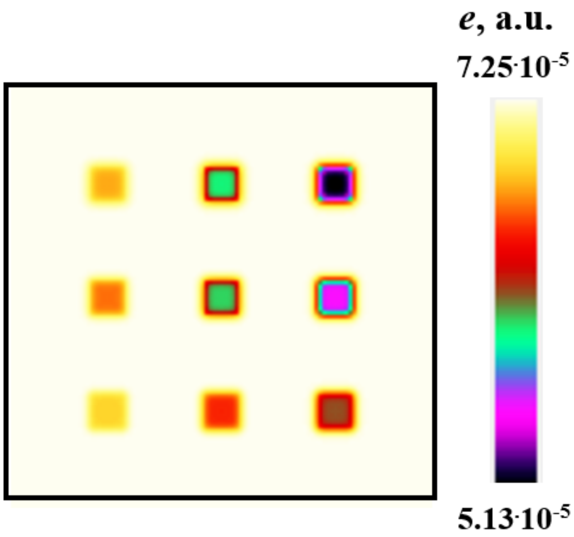

Fig.2b Effusivity map (1 mm-thick CFRP sample)

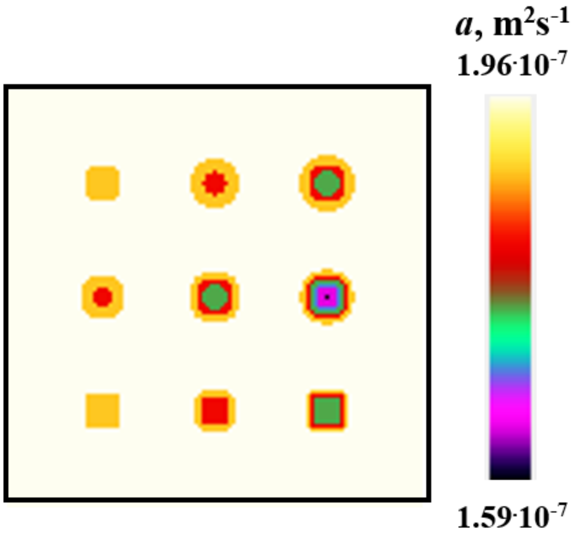

Fig.2c Diffusivity map (6 mm-thick CFRP sample).

Fig.2 Test model for analyzing relationship between defect parameters and local variations of effusivity/diffusivity (all defects 10×10 mm):

3.2 Modeling results and discussion

All results are presented in Table1 where relative variations (in percent) of effusivity and diffusivity are given for each particular defect (36 test cases in total). The same results are graphically shown in figure3. Notice that there are no results for the defects at the depth 0.8 mm in the 1 mm-thick sample because of the so-called inversion phenomenon. The concept of this phenomenon is that, in a two-sided procedure, the defects located close to the rear surface first produce negative temperature signals (defect areas are colder than the background) and then become positive thus making the corresponding values of diffusivity variations in Table 1 “non-uniform” (these values are specified with **). The inversion phenomenon deserves further exploration.
In fact, the obtained relationships qualitatively repeat those which take place for differential signals, namely, relative effusivity variations decay linearly with depth and increase linearly with defect thickness, while diffusivity variation is maximal for the defects located in the middle of the sample, and the corresponding relationships $\Delta a/a\ (l)$are close to linear.

4. Experimental illustration

The theory above was illustrated by evaluating a CFRP sample with thickness of 4.7 mm subjected to a standard impact damage test characterized by the energy of 60 J and velocity of 7 m/s (Figure 4a).The sample was tested on both F- and R-surfaces performing one- and two-sided tests to produce 4 sets of the IR image sequences, which were analyzed for variations of apparent effusivity and diffusivity. The sample was heated with 2 flash tubes (6.4 kJ energy in total, 5 ms pulse duration). On the F-surface, the impact damage was hardly detected (the so called Barely Visible Impact Damage-BVID), while the major delaminations appeared on the R-surface in the well-known “butterfly” form (see figure 4a). It is worth noting that, unlike the theoretical cases analyzed above, an impact damage defect represents a complicated conglomerate of delaminations and cracks located at different depths and oriented along the fiber direction. Often, a main body of impact damage appears closely to the sample rear surface.

Table.1 Effusivity/diffusivity variations over air-filed defects
in 1 and 6 mm-thick CFRP samples (model from Fig. 2)

Defect depth l, mm	Defect thickness d, mm	One-sided procedure $\lvert \Delta e/e \rvert$, % *	Two-sided procedure $\lvert \Delta a/a \rvert$, %
1 mm-thick sample			
0.2	0.05	32.4	21.1
	0.10	44.4	34.6
	0.15	51.3	40.0
0.5	0.05	16.9	28.6
	0.10	25.1	44.3
	0.15	29.6	48.1
0.8	0.05	5.50	21.1**
	0.10	10.1	21.1**
	0.15	14.7	11.9**
6 mm-thick sample			
1	0.05	11.5	3.6
	0.10	18.0	7.1
	0.20	27.1	10.7
3	0.05	3.1	7.1
	0.10	5.9	10.7
	0.20	9.6	15.8
5	0.05	0.96	3.6
	0.10	1.3	7.1
	0.20	2.3	10.7

* These values are determined for the times when the differential temperature signals over particular defectsbecome maximal.

** These values correspond to a special case where temperature signals on the rear surface experience the so-called inversion, i.e. change the sign.

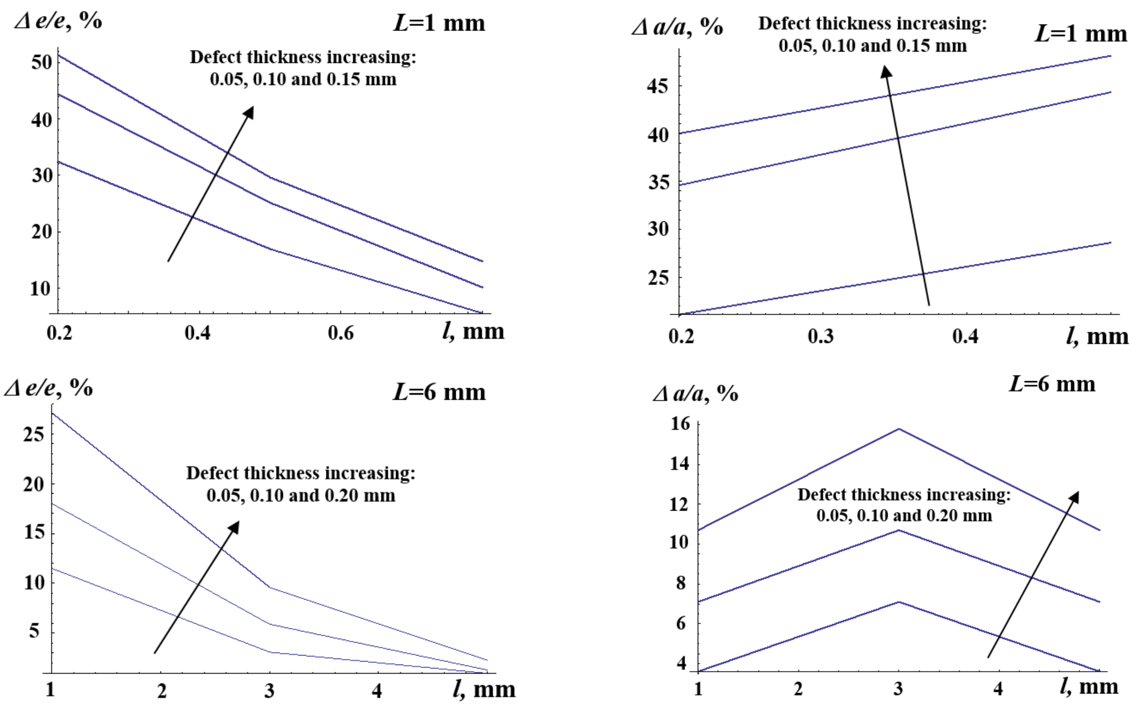

Fig.3 Effusivity/diffusivity variations over air-filled defects
in 1 and 6 mm-thick CFRP samples (data from Table 1)

The evolution of the F-surface temperature distribution over the impact damage in a one-sided test procedure is shown in figure 4b. It is seen that immediately after the heat pulse one can see the thin superficial delamination while the main body of the defect appears later. The analysis of the in-depth structure of impact damage defects is beyond the scope of this study; the use of dynamic thermal tomography for 3D reconstruction of impact damage was discussed in [11].

Figure 4c shows the evolution of signal-to-noise ratio (SNR) through the recorded source image sequencethatwasroutinely calculated for defect (D) and non-defect (ND) areas chosen by the operator. It follows that the defect can be detected best of all at about 1 s. Then the source sequence was converted into the sequence of apparent effusivity images according to Eq. (3).

The corresponding $e(\tau)$ plot is presented in figure 4d to illustrate that immediately after the heat pulse the effusivity magnitude in the chosen (D and ND) areas is the same, and a noticeable difference occurs in the interval from 0.4 to 4 s. An F-surface map of $e(i,j)$is shown in figure 4e to illustrate 19 % variation of thermal effusivity over the impact damage. It is worth reminding that $e(\tau)$values vary in time and an absolute value of $\Delta e/e\ (\tau)$ reaches maximum at a particular time (at about 1s in figure 4e).

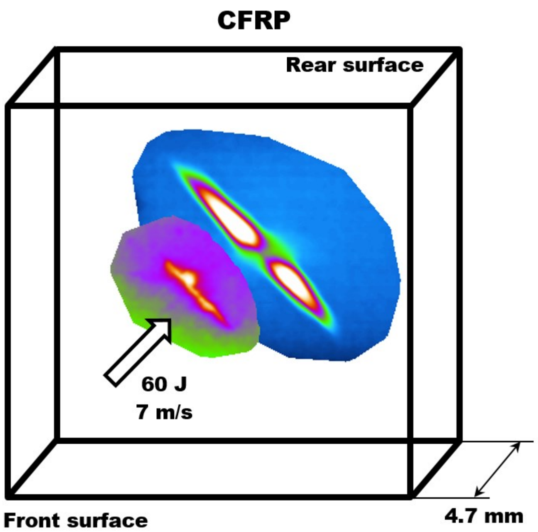

Fig.4a Test scheme and examples of temperature distributions on F- and R-surfaces

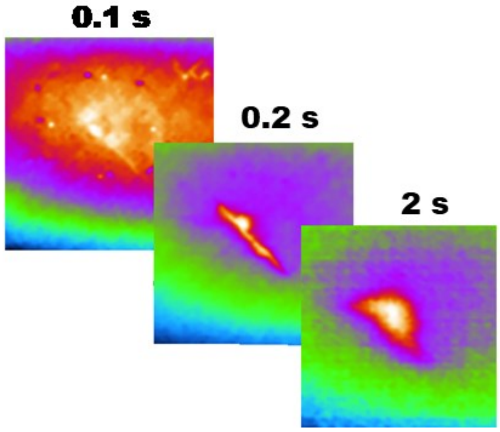

Fig.4b F-surface temperature evolution

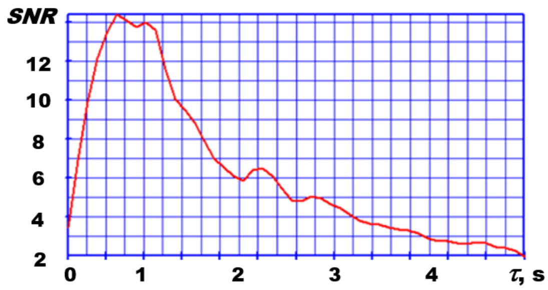

Fig. 4c SNR vs time

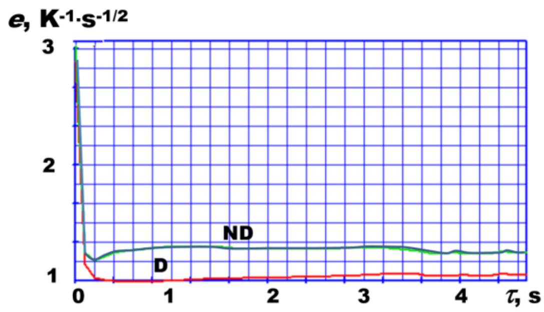

Fig.4d Effusivityvs time in defect (D) and non-defect (ND) areas

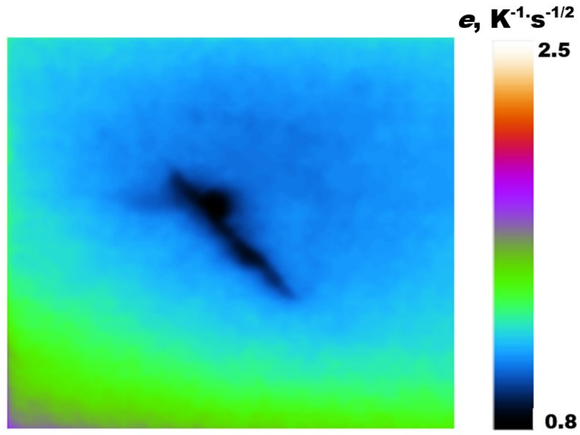

Fig.4e Effusivity map at 1s (19 % effusivity variation over impact damage)

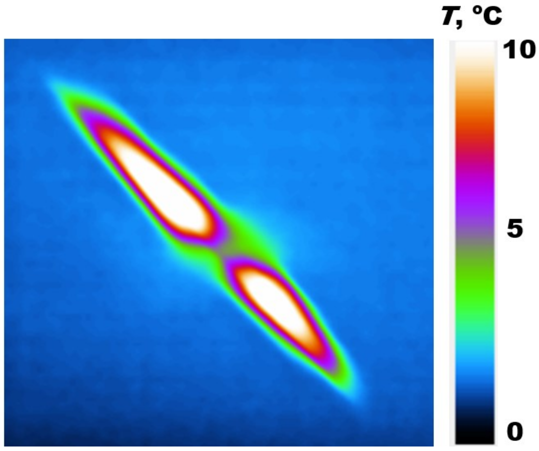

Fig.5a R-surface temperature distribution at 2.6 s

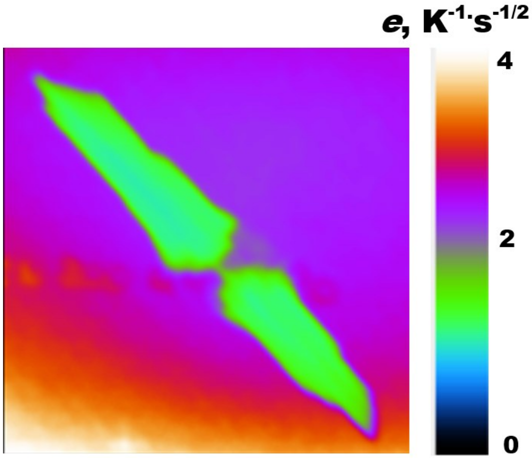

Fig.5b Eeffusivity map at 2.6s (42% effusivity variation over impact damage)

Fig.5 Evaluating R-surface effusivity in a one-sided test procedure (pulsed heating of 4.7 mm-thick CFRP sample subjected to 60 J impact

In a one-sided test procedure, the sample excess temperature T reached 10°C, and the defect was clearly seen on the R-surface in the "butterfly" form (Fig. 5a). This means that the main body of the impact damage located closely to the R-surface to produce effusivity variation of 42 % (Fig. 5b). The results in Fig. 4 and 5 prove that one-sided values of effusivity are strongly dependent on time and defect depth.

In the two-sided procedure of diffusivity measurement, first, the F-surface was heated, and the R-surface temperature was captured (figure 6a). The temperature profiles were of the classical Parker shape (see figure 6b), and the respective diffusivity image is presented in figure 6c. In non-defect areas, the composite diffusivity was $(3\text{-}3.5)\cdot10^{-7}$ $m^2\cdot s^{-1}$, that is a typical value for CFRP composite, while over the defect it dropped down to $(2\text{-}2.4)\cdot10^{-7}$ $m^2\cdot s^{-1}$. The average diffusivity variation over the defect was about 44 %.

In the case of heating the R-surface and determining diffusivity on the F-surface, the results were very similar to those on the R-surface (Figure 7, diffusivity variation 43 %) that is explained by the known fact that material diffusivity measurements are independent on which surface is heated and which - monitored. By other words, two-sided thermal NDT tests are preferable if defects might be located at any depth.

The experimental results obtained for the impact damage defect, which is characterized by a complicated structure of single delaminations, demonstrate that relative variations of thermal properties are of the same order of magnitude as it appears in the case of a theoretical model containing single air-filled defects.

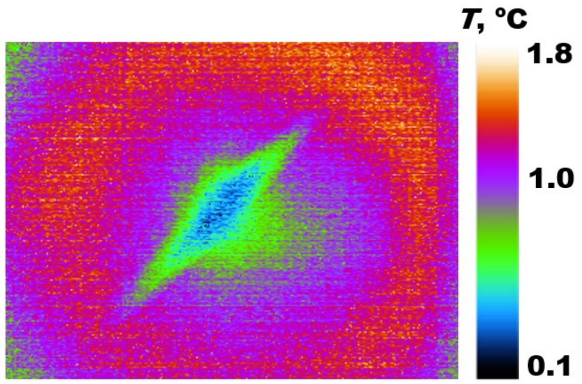

Fig.6a R-surface temperature distribution at 10s

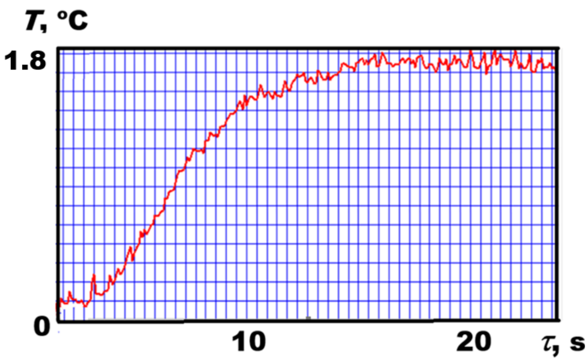

Fig.6b R-surface temperature evolution in time

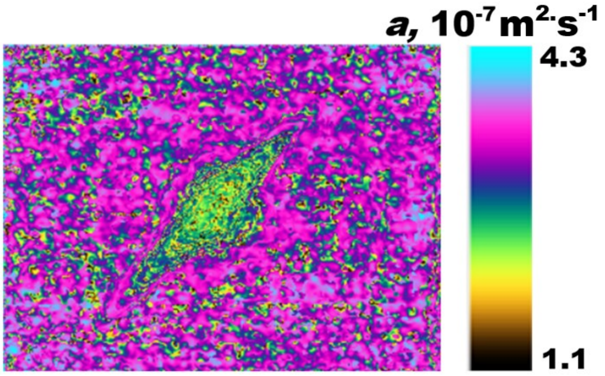

Fig.6c R-surface diffusivity map (diffusivity variation over defect 44 %)

Fig.6 Evaluating R-surface diffusivity in a two-sided test procedure (pulsed heating of 4.7 mm-thick CFRP sample subjected to 60 J impact)

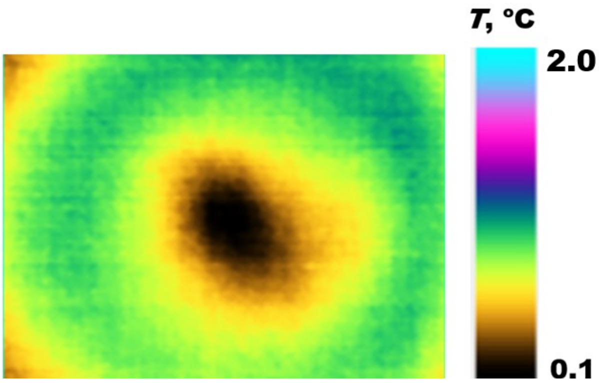

Fig.7aF-surface temperature distribution at 10 s

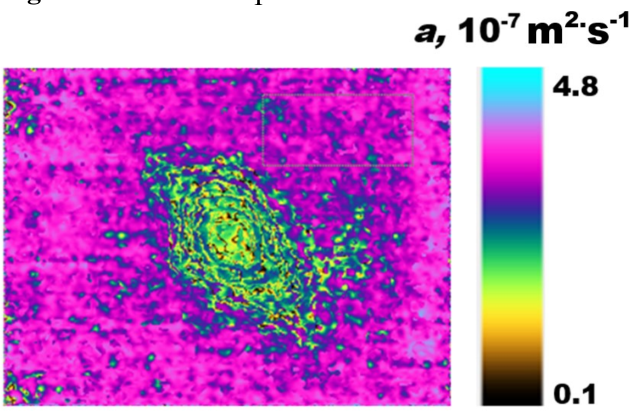

Fig.7b F-surface diffusivity map (diffusivity variation over defect 43 %)

Fig.7 Evaluating F-surface diffusivity in a two-sided test procedure (pulsed heating of 4.7 mm-thick CFRP sample subjected to 60 J impact)

5 .Conclusions

➢ In one-sided thermal NDT procedures, the effusivity parameter can be used for characterizing hidden defects. Effusivity magnitude depends on defect depth thus allowing defect depth evaluation, mainly, for subsurface defects. The main disadvantages of this technique are as follows: 1) an image sequence cannot be replaced with a single image of effusivity, because effusivity estimates vary in time, 2) effusivity variations in defect areas strongly decay with defect depth, 3) effusivity is linearly related to absorbed energy.

➢ Over subsurface defects, apparent local effusivity variation linearly decays with defect depth and increases with defect thickness.

➢ In two-sided thermal NDT procedures, the modified Parker method is recommended for evaluating diffusivity distributions. This technique is implemented in the time domain that ensures its better noise resistance compared to effusivity measurements that are fulfilled in the temperature domain.

➢ Over subsurface defects, local diffusivity variation reaches maximum in the middle of the sample and increases linearly with defect thickness.

➢ A 60 J impact damage in a 4.7 mm-thick CFRP sample is characterized by effusivity variations from about 20 to 40 % and diffusivity variations of about 40 %.

➢ The future research will be devoted to the analysis of whether relative variations of composite effusivity/diffusivity can be used for evaluating defect parameters.

6. References

[1] Vavilov V., Burleigh D. (2020), “Infrared thermography and thermal nondestructive testing”, Springer Nature Switzerland, DOI: 10.1007/978-3-030-48002-8.

[2] Bing W., Shuncong Z., Tung-Lik L., Fancey K.S., JiaweiMi (2020), “Non-destructive testing and evaluation of composite materials/structures: A state-of-the-art review”, Adv. in Mech. Eng., 12 (4), pp. 1-28.

[3] Chulkov A.O., Sommier A., Pradere C., Vavilov V.P., Siddiqui A.O., Prasad Y.L.V.D. (2021), “Analyzing efficiency of optical and THz infrared thermography in nondestructive testing of GFRPs by using the Tanimoto criterion”, NDT & E Intern., vol. 117, 102383. DOI: 10.1016/j.ndteint.2020.102383.

[4] Mulaveesala R., Rani A., Kher V., Mishra P., Kaur (2021), "J. Infrared non-destructive testing and evaluation for inspection of carbon fiber reinforced polymer materials", Proc. Thermosense: Thermal Infrared Applications XLIII conf., vol. 11743, 117430Q, DOI: 10.1117/12.2593390.

[5] Dua G., Arora V., Mulaveesala R. (2018), "An aperiodic digitized frequency modulated thermal wave imaging for testing and evaluation of carbon fiber reinforced polymer materials", JNDE, 16 (12), pp. 30-32.

[6] Vavilov V., Chulkov A., Smotrov A., Smotrova S., Moskovchenko A. (2019), "Characterizing impact damage in GFRP/CFRP composites by determining thermal effusivity/diffusivity", Measurement Science and Technology, vol. 30, 034003, DOI: 10.1088/1361-6501/ab018e.

[7] Vavilov V.P., Chulkov A.O., Smotrova S.A., Smotrov A.V., Scherbakov V.N., Storozhenko V.A. (2022), "Infrared thermographic analysis of thermal property variations in composites subjected to impact damage, thermal cycling and moisture saturation",. Composite Structures, vol. 296, 115927, DOI: 10.1016/j.compstruct.2022.115927

[8] Zalameda J.N., Winfree W.P. (2004), "Improved sampling of thermal transients using Focal Plane Array infrared imagers", Proc. Thermosense: Thermal Infrared Applications XXVI conf., vol. 5405, pp. 374-381.

[9] Winfree W.P., Zalameda J.N. (2002), "Single sided thermal diffusivity imaging in composites with a shuttered thermographic inspection system", Proc. Thermosense: Thermal Infrared Applications XXIV conf., vol. 4710, pp. 536-544.

[10] Parker W.J., Jenkins R.J., Butler C.P., Abbot G.L. (1961), "Flash method of determining thermal diffusivity, heat capacity and thermal conductivity", J. of Appl. Phys., vol. 32, pp.1679-1684.

[11] Vavilov V.P., Shirayev V.V., Kuimova M.V. (2018), "Time- and phase-domain thermal tomography of composites", Photonics, 5 (4), pp. 31-42. DOI: 10.3390/photonics5040031.